Millimeter-Precision Ultrasonic DSSS Positioning Technique With Geometric Triangle Constraint

Ishii, Toru
Yasuda, Yuto
Sato, Shun
Izumi, Shintaro
Kawaguchi, Hiroshi

(Citation)
IEEE Sensors Journal,22(16):16202-16211

(Issue Date)
2022-07-11

(Resource Type)
journal article

(Version)
Accepted Manuscript

Millimeter-Precision Ultrasonic DSSS Positioning Technique with Geometric Triangle Constraint

ISHII Toru, Yuto Yasuda, Shun Sato, Shintaro Izumi, *Member, IEEE*, and Hiroshi Kawaguchi, *Member, IEEE*

***Abstract*— In this paper, we present a 3-D ultrasonic measurement technique that uses direct sequence spread spectrum (DSSS) with simultaneous multiple code-division multiple access (CDMA) signals. This technique can be applied in precise indoor locating systems. By placing three microphones close to one another separated by distances on the order of the ultrasound wavelength and imposing the constraint that one transducer and two from the three microphones form three triangles in the space (i.e., the triangle constraint) for 3-D ultrasonic DSSS trilateration measurement, millimeter 3-D positioning precision is achieved. The experimental results for a positioning system comprising a set of three microphones and four ultrasound transducers, each of them transmitting its respective 256-bit DSSS code, demonstrate that the proposed system can measure the spatial 3-D location of the receiver with a standard deviation of less than 1.21 mm. The proposed technique is suitable for potential future indoor positioning system (IPS) applications that require sub-centimeter 3-D positioning.**

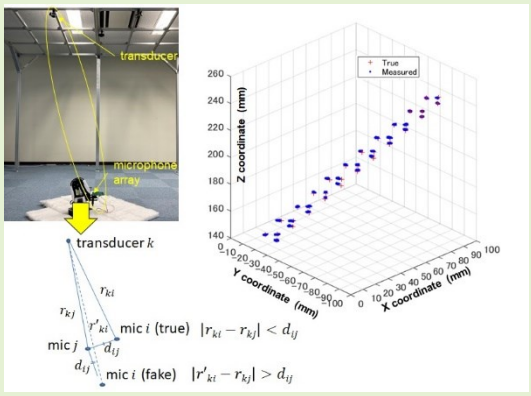

***Index Terms*— CDMA, DSSS, M–sequence, Time of flight, Ultrasound**

I. Introduction

A number of ultrasound measurement systems for precise indoor positioning systems (IPS) with accuracies higher than 10 cm have been reported [1]. The accuracy of these systems is generally better than that of other systems such as computer vision or radio wave beacons. To measure the time of flight (TOF) of the signal from the transmitter to the receiver with even higher precision than that achieved in conventional ultrasound measurements using amplitude pulses, the ultrasonic direct sequence spread spectrum (DSSS) with the maximum length sequence (M-sequence) or other similar pseudo-random noise codes have been used in more than a dozen studies reported over the past two decades [2–20].

DSSS is a technique that increases the signal bandwidth by multiplying a wideband spreading signal, such as an M-sequence, with a data-modulated signal to increase the robustness of the signal against noise and interference [21]. Owing to its inherent characteristics, such as pseudo-random noise, ultrasonic DSSS positioning has advantages in terms of precision and robustness. Another advantage of DSSS is that it enables the use of code division multiple access (CDMA) in which multiple transmitters send their respective codes simultaneously to increase the measurement rate of the system. Hazas *et al.* developed an ultrasound DSSS positioning system called Dolphin using a wideband piezo film as both the transmitter and receiver [2, 3]. They evaluated the system using two modes. In the centralized mode, the transmitter is attached to a mobile node, and its position is measured by the central system. In the privacy-oriented mode, the mobile node receives a measurement signal and calculates its own location. The positioning accuracies within a 95% confidence level for each mobile unit of the CDMA system in the former and latter modes were 2.2 and 4.9 cm, respectively [3]. Prieto *et al.* achieved positioning errors of less than 1 cm within a 90% confidence level in a privacy-oriented CDMA configuration in their system called 3-D LOCUS using wideband omnidirectional transducers and calibrating the ranging errors caused by the directivity of the transducer and system delays [4, 5]. Sertatil *et al.* reported an accuracy of 2 cm within a 99% confidence level in their privacy-oriented CDMA system consisting of commercially available low-cost audio tweeters [6]. They proposed selecting the three most reliable correlation signals for the positioning calculation and demonstrated the effectiveness of the approach, particularly for shorter-length codes, although they did not evaluate its effectiveness quantitatively. Perez *et al.* evaluated the positioning errors of several DSSS codes [7]. They showed that the positioning errors of DSSS-CDMA are significantly affected by interference, including multipath

This study is based on results obtained from a project commissioned by the New Energy and Industrial Technology Development Organization (NEDO). The corresponding author is ISHII Toru (e-mail: ishii_toru@cs28.cs.kobe-u.ac.jp). He and Hiroshi Kawaguchi (e-mail: kawapy@godzilla.kobe-u.ac.jp) are with the Graduate School of Science, Technology, and Innovation at Kobe University, Kobe 6578501, Japan. Yuto Yasuda (e-mail: yasuda.yuto@cs28.cs.kobe-u.ac.jp) and Shintaro Izumi (e-mail: shin@cs28.cs.kobe-u.ac.jp) are with the Graduate School of System Informatics, Kobe University, Kobe 6578501, Japan. Shun Sato (e-mail: shin@cs28.cs.kobe-u.ac.jp) is with Computer Science and Systems Engineering, Kobe University, Kobe 6578501, Japan.

interference, which varies from point to point in the space. Seco *et al.* improved the CDMA accuracy of 3-D LOCUS by adding parallel interference cancellation (PIC) and inter-symbol interference compensation (ISI) to the system [8]. They obtained the excellent result of 0.90 mm for the CDMA positioning error within a 90% confidence level when both PIC and ISI were applied [9]. Medina *et al.* reported standard deviation of less than 0.3 mm in 1-D ranging and of 3.8 mm in 3-D positioning using their quadrature detector [10]. Seco *et al.* showed that the number of outliers, defined as errors larger than two signal wavelengths, was significantly reduced by PIC and ISI [8, 9], but none of the aforementioned DSSS-CDMA systems analyzed the root cause of the outliers. Another study proposed applying the triangle inequality to filter out outliers [11, 12]. However, neither [11] nor [12] could detect sub-centimeter errors because the perimeter length of the triangles in either study, which limits the error detection resolution, was larger than 20 cm. In this study, a novel positioning technique with millimeter precision was developed by applying the triangle constraint with a perimeter of less than 1 cm, using three closely aligned microelectromechanical system (MEMS) microphones. The experimental result of 3-D precision had a standard deviation of less than 1.21 mm in the 0.1 m × 0.1 m × 0.1 m evaluation region with no reflective walls nearby and of less than 9.40 mm in the 0.2 m × 0.2 m × 0.105 m region within a mocked room corner made of three panels. The proposed technique is suitable for future indoor positioning applications in which precise autonomous control is required, such as drones or robots in houses, factories, and other common indoor environments.

The remainder of this paper is organized as follows. The causes of the large positioning errors found in our evaluations are analyzed in Section II. The proposed technique is described in Section III. The experimental results are presented in Section IV. Finally, the conclusions are presented in Section V.

II. Problems In Ultrasonic Dsss Positioning

In ultrasonic DSSS ranging/positioning systems, the cross-correlation (*CC*) between the transmitted (*Tx*) and received (*Rx*) signals is first calculated, and the position of the most prominent peak in the correlation along the time axis is determined and considered as the TOF. The CC is expressed by the following equation:

$$CC(j) = \sum_{i=1}^{K} \left(Tx(i) \cdot Rx(j+i-1) \right). \qquad (1)$$

where i and j represent the indices of *Tx* and *Rx*, respectively, and K is the length of *Tx*. The time resolutions of i and j are determined by the sampling frequency of *Rx* of the system. Because the theoretical time resolution of wideband systems is limited by the Cramér–Rao lower bound, which is determined by the signal-to-noise ratio (SNR) and carrier frequency of the system [22], the ranging resolution of the DSSS can be enhanced up to this limit by setting a higher sampling frequency. Therefore, it is possible to achieve a ranging resolution less than the carrier wavelength when a sufficient SNR is obtained.

Ideally, *CC* should have the same signal as the auto-correlation of *Tx* with only a single sharp peak, similar to the δ function. However, in the real world, *CC* is distorted by the limited bandwidth of the system, particularly that of the ultrasound transducer, as well as by interference with other signals present in the field. Fig. 1 shows examples of the actual cross-correlation signals from our previous study [20] at two different receiver locations. The plotted lines are the *Tx–Rx* cross correlations in the first iteration of 100 consecutive measurements, whereas the circles in the figure show the maximum peaks in each of the 100 measurements.

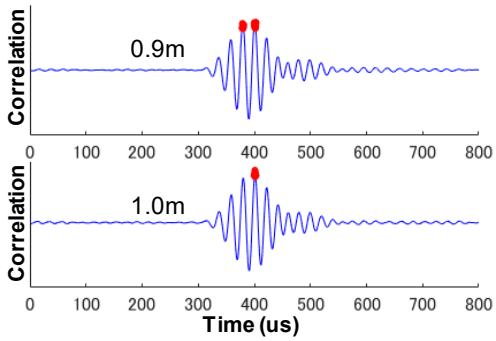

Fig. 1. Cross-correlation between the transmitted and received signals of an M-sequence code. Alternations of the maximum peak were observed at 0.9 m, whereas the maximum peaks were all located at the same peak throughout 100 measurements at 1.0 m.

At 0.9 m, the maximum peak position alternated from time to time between the two adjacent peaks. The difference between the intensities of these two peaks was sufficiently small, and the maximum peak positions did not always exhibit the true distance. In contrast, all the maximum values were confined to the same peak at 1.0 m. We call the problem at 0.9 m λ leap, as the span between two adjacent peaks corresponds to the carrier wavelength (λ) in the distance. In our previous study, we reported that considering the envelope peak can mitigate the error deviation caused by λ leap [20]. Besides the λ leap, the problem of multipath interference may occur if there are objects that reflect the ultrasound signal somewhere near either the transmitter or the receiver. Fig. 2 shows the *Tx–Rx* cross-correlations from our experiment, which are described in Section IV. Fig. 2(a) shows the cross correlation of transducer

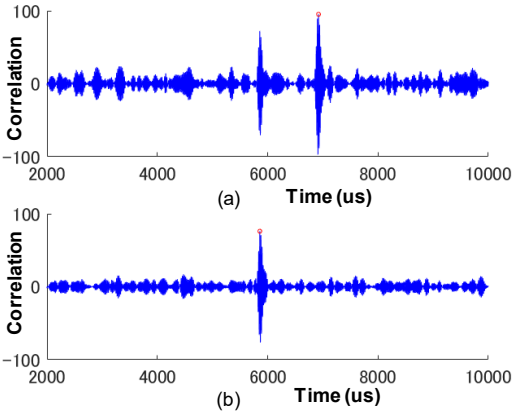

Fig. 2. (a) Multipath reflection from the floor generated a ghost peak that was higher than the direct path peak at a particular location in the space. (b) Only the direct path peak was observed when the floor was covered with a sound absorbing cloth.

II's *Tx* and mic 2's *Rx* in Fig. 7(a), and Fig. 2(b) shows that in Fig. 6(a). In Fig. 2(a), the highest peak, which is marked with a circle, occurs not at the distance of the direct path but rather at that of the path reflected from the room floor. Fig. 2(b) shows the *Tx–Rx* cross correlation when the transmitter and receiver were set at exactly the same positions as in Fig. 2(a), and a sound-absorbing synthetic cotton fiber was laid on the floor. A prominent peak was observed only for the direct path, as shown in Fig. 2(b).

In 3-D TOF positioning systems, the spatial coordinates of one receiver are calculated based on the measured distance between the receiver and three or more transmitters. The presence of a λ leap or multipath interference in one or more paths leads to a larger dispersed error that exceeds the distribution error range of the *Rx* sampling frequency of the system.

III. Theory

A. Trilateration Calculation

The microphone's coordinates (x, y, z) can be calculated by solving (2).

$$r_k = \sqrt{(x - X_k)^2 + (y - Y_k)^2 + (z - Z_k)^2} \quad (k = 1,2, \dots, N), \tag{2}$$

where r_k and (X_k, Y_k, Z_k) represent the measured distance between the microphone and transmitter k and the transmitter's coordinates, respectively. N is the total number of transmitters. Nonlinear (2) can be solved by the pre-known iterative process explained in [23]. In this process, the coordinates (x^j, y^j, z^j) in iteration time j are renewed using the following equation:

$$\begin{pmatrix} x^{j+1} \\ y^{j+1} \\ z^{j+1} \end{pmatrix} = \begin{pmatrix} x^j \\ y^j \\ z^j \end{pmatrix} + \begin{pmatrix} \Delta x^j \\ \Delta y^j \\ \Delta z^j \end{pmatrix}. \tag{3}$$

The increments $(\Delta x^j, \Delta y^j, \Delta z^j)$ are obtained by solving (4):

$$\frac{\partial r_k}{\partial x}\Delta x^j + \frac{\partial r_k}{\partial y}\Delta y^j + \frac{\partial r_k}{\partial z}\Delta z^j = r_k - r_k^j \quad (k = 1,2, \dots, N), \tag{4}$$

where $\frac{\partial r_k}{\partial x}, \frac{\partial r_k}{\partial y}, \frac{\partial r_k}{\partial z}$ are given by partial differentiation of (2) as follows:

$$\frac{\partial r_k}{\partial x} = \frac{x - X_k}{r_k}, \quad \frac{\partial r_k}{\partial y} = \frac{y - Y_k}{r_k}, \quad \frac{\partial r_k}{\partial z} = \frac{z - Z_k}{r_k}. \tag{5}$$

When N is greater than 3, the conventional least-squares algorithm [24] is applied to solve (4).

The ranging error propagation to positioning errors is also calculated by (4) by substituting the positioning errors $(\Delta x_e, \Delta y_e, \Delta z_e)$ for $(\Delta x^j, \Delta y^j, \Delta z^j)$, and the ranging error Δr_e for $r_k - r_k^j$, respectively.

B. Proposed Technique

The proposed technique consists of two signal processing stages. The first stage is called unreliable data discarding (UDD), which was originally proposed by Sertatil *et al.* [6]. Here, among the four transmitters, the transmitter that shows the lowest *Tx–Rx* correlation peak is discarded, and the remaining three transmitters are used for the positioning calculation. This process was applied to each *Rx* independently. The first purpose of this stage is to improve the precision, as in the original work of Sertatil *et al.*, and the second is to reduce the computational workload in the next stage. The next stage is the triangle-constraint method. Zhao and Wang proposed this method to reject an outlier that is highly probable to be a reflected signal [11].

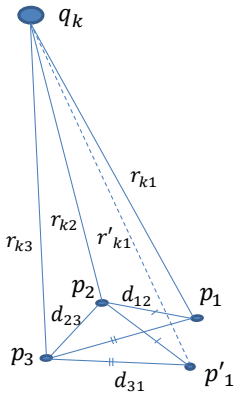

Fig. 3. Principle of the proposed triangle constraint technique: the true peak candidates in each *Tx–Rx* cross-correlation are selected so that the ranges r_{ki} and r_{kj}, which are determined by the chosen peaks, form two peripherals of the triangle $p_i\, p_j\, q_k$.

In our method, three receiver microphones separated from one another by distances of the order of λ were used. Fig. 3 illustrates the principle of this method. In the figure, q_k represents the position of a particular transmitter in the space, where k is the index of the transmitter, and p_1, p_2, and p_3 are the positions of the three microphones, mic 1, mic 2, and mic 3, respectively, with predetermined relative geometric relationships. These three microphones may correspond to three MEMS microphones mounted on the surface of a printed circuit board (PCB).

r_{ki} represents the true distance between q_k and p_i, whereas r'_{k1} is the false distance for r_{k1} derived from the λ leap. p'_1 represents the fake position of mic 1, determined by r'_{k1}. d_{ij} is the distance between p_i and p_j. Because p_i, p_j, and q_k form a triangle in the space and d_{ij} is a known value, r_{ki} and r_{kj} must satisfy inequality (6):

$$|r_{ki} - r_{kj}| < d_{ij} \quad (i, j = 1,2,3,\ i \neq j). \tag{6}$$

To address the λ leap, not only the highest but also the second-highest peak in the cross-correlation function is selected and examined if it satisfies inequality (6). Therefore, even when r_{k1} does not show the highest peak, it remains a candidate as long as the combination of r_{k1} and its corresponding r_{kj} $(j = 2, 3)$ satisfies inequality (6). Regarding candidate selection, it is possible to limit the candidates to only r_{k1} by setting either one of d_{1j} $(j = 2, 3)$ to be shorter than 0.5λ. This is because r'_{k1}, which differs from r_{k1} by λ, makes $|r'_{k1} - r_{kj}|$ exceed 0.5λ if $|r_{k1} - r_{kj}| < 0.5\lambda$ is always true. However, we set d_{12} and d_{23} to 1.03λ (7 mm) and d_{31} to 1.45λ (9.9 mm), respectively, for the following reasons. First, this avoids the interference problems

that may result from either the λ leap or multipath interference when the microphones are placed too close together. Second, there is a limitation in the physical size of the components on the microphone array PCB (mic-array PCB), although there is room for improvement by employing higher-density circuit design/mounting techniques such as multi-layer PCBs. This distancing optimization will be a major topic for future work. By selecting more than two peaks from the cross-correlation, it is possible to apply the same candidate-selection process to overcome the multipath interference problem. This process is performed for each transmitter q_k and all possible combinations of r_{ki} are stored. Finally, if two or more combinations remain as candidates, the most appropriate combination from among all the candidates at each q_k is determined based on the sum of the peak values in each combination. If four peaks are selected for each microphone, which is the evaluated condition in the next section, the maximum possible number of combinations is $4 \times 4 \times 4 = 64$. Therefore, the computational complexity increases owing to the triangle constraint under this condition, which is expressed as follows:

Subtract, Absolute: $3 \times 64 = 192$ (inequality (6)),

Add: $2 \times 2 = 4$ (sum of the peaks of the last two candidates),

Compare: $3 \times 64 + 1 = 193$ (inequality (6), the last two candidates).

Suppose that above, the cost of each arithmetic operation is one, and the total cost increase is 389 for the coordinates of the three microphones. However, this increase is negligible compared to the cross-correlation calculation defined by (1), where K^2 multiply and accumulate (MAC) operations are required, which amounts to 2.36×10^8 MAC operations per microphone under the condition given in Table II in the next section.

IV. Evaluation

A. Evaluation System

The results of the evaluation are presented in the following section. Figs. 4 and 5 show the experimental environment and block diagram of the experiment, respectively. In the evaluation

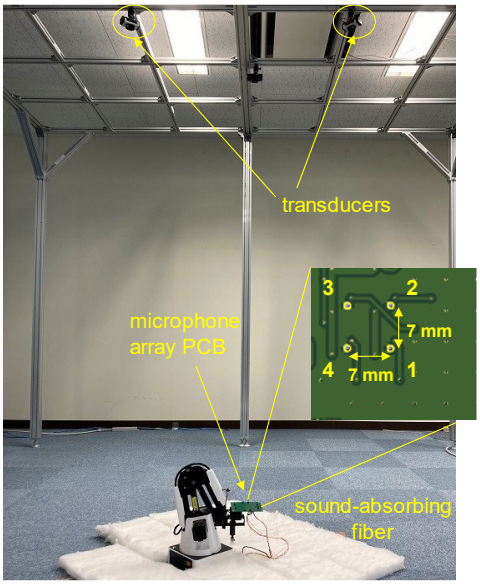

Fig. 4. Experimental environment.

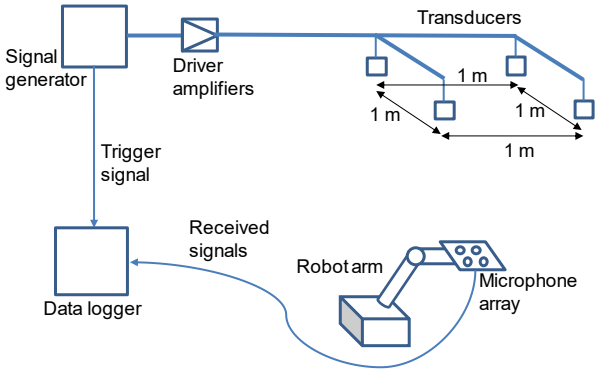

Fig. 5. Equipment setup.

system, four DSSS-coded signals were generated by a binary pattern signal generator, amplified by driver amplifiers, and finally output simultaneously as ultrasound *Tx* signals every 40 ms from four transducers I–IV placed 2.08 m above the floor.

The amplifier output amplitude was 20 Vpp and the carrier frequency of the *Tx* signals was 50 kHz. In addition to the coded signals, the trigger signal for the start timing of the *Tx* was synchronously outputted from the signal generator to a data logger. Four MEMS microphones (mics 1–4) were mounted to form the four vertices of a 7 mm × 7 mm square on the mic-array PCB. The mic-array PCB was attached to the edge of the robot arm, and the signals received by the microphones were stored using a data logger. Sound-absorbing synthetic cotton fibers were laid on the floor around the robot arm. The major equipment components are listed in Table I.

TABLE I
MAJOR COMPONENTS OF THE EXPERIMENT

Component	Part no. (Manufacturer)
Transducer	480EP900 (Pro-Wave)
Microphone	SPU0410LR5H-QB (Knowles)
Data logger	MR6000 (Hioki)
Robot arm	Dobot Magician (Shenzhen Yuejiang Technology)

TABLE II lists the properties of the signals and equipment setup used in the experiment. The four 255-bit M-sequence codes that showed the least cross-correlation with one another

TABLE II
SIGNAL AND EQUIPMENT PROPERTIES

Signal property	Value
DSSS code length	255
Carrier wave cycles per bit	3
DSSS code	M-sequence
Modulation	BPSK
Carrier wave frequency	50 kHz
Measurement interval	40 ms
Sampling frequency	1 MHz
Microphone size	3.76 mm × 3.0 mm
Microphone directivity	omnidirectional
Transducer size	36.6 mm × 26.6 mm
Transducer beam angle (−6dB)	19° × 38°
Transducer coordinates (mm)	I (484, 530, 2080) II (484, −470, 2080) III (−516, −470, 2080) IV (−516, 530, 2080)

in our preliminary calculations were selected as the four *Tx* codes from among the 16 possible candidates.

B. Evaluation I: λ Leap

First, we evaluated the effect of the proposed technique on the λ leap. For this evaluation, the mic-array PCB was fixed at the origin of the robot arm, where the λ leap was observed at two microphones in the conventional independent single-microphone measurement. The robot arm was placed such that the distances from the origin to the four transducers were approximately equal. The floor around the robot arm was covered with sound-absorbing fiber. The coordinates of each microphone were calculated by solving trilateration equations. A total of 124 measurements were taken using the conventional independent single-microphone measurement with four transducers (Conventional), unreliable data discarding (UDD), and unreliable data discarding followed by triangle constraint (UDD + Triangle). The results are shown in Figs. 6(a), (b), and (c). The true positions marked by '+' in the figures were obtained at the calibrated position of mic 1. They matched the mean location values determined from mic 1 in Fig. 6(b) after it was confirmed that neither λ leap nor multipath errors were present in the final positioning results obtained at the position of mic 1. The arrows I–IV indicate the direct paths from the corresponding transducers to mic 1. In Fig. 6(a), where the least-squares algorithm using all four transmitters that minimizes the nonlinear cost function [24] is applied, constant offset errors were observed at 1. While the errors at mic 1 were mitigated by considering envelope peaks (measured (envelope)), the triangular shape formed by mics 2, 3, and 4 was distorted. In Fig. 6(b), dispersed errors due to the λ leap are present for mic 4, although they are not observed for mics 1, 2, and 3. In the triangle constraint process shown in Fig. 6(c), the candidate selection and determination of the most suitable combination explained in the previous section were applied to the cross-correlation data obtained from the UDD process shown in Fig. 6(b). All possible combinations of three microphones that form the vertices of a triangle, that is, (1, 2, 3), (2, 3, 4), (3, 4, 1), and (4, 1, 2), were evaluated. The plotted points numbered '*j*' exhibit the measured results of microphone *j* from the group (*i*, *j*, *k*). For example, points '4' were obtained from the result of (3, 4, 1).

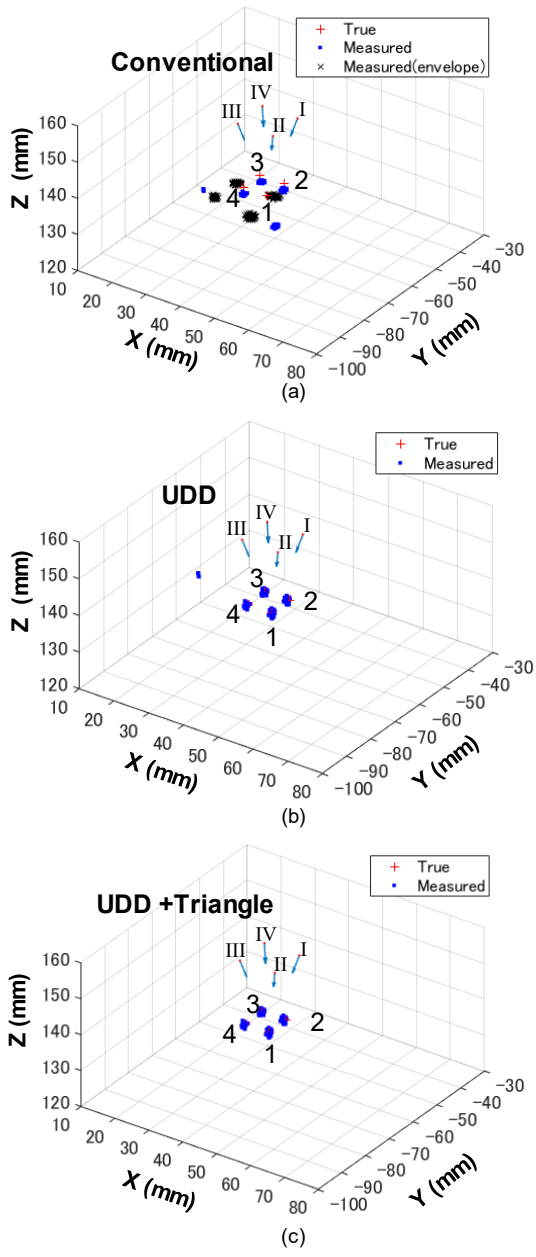

Fig. 6. Evaluation I: λ leap. In the Conventional case shown in (a), dispersed errors for mics 1 and 4 were observed. In the UDD case shown in (b), the dispersed errors for mic 1 disappeared while those for mic 4 appeared at different positions. In the UDD + Triangle case in (c), no dispersed errors were observed at all four mics.

Table III lists the location errors shown in Fig. 6. One interesting result is that mic 1 in Conventional exhibited a much larger mean error than the other microphones, but its standard deviation was as small as those of mics 2 and 3, for which no large errors were observed. This implies that the *Tx–Rx* cross-correlation of mic 1 and the transducer that was rejected in the UDD process showed a constant single λ leap from the true distance throughout all 124 measurement iterations.

TABLE III
LOCATION ERRORS IN EVALUATION I: LAMBDA LEAP

Mic.	Conventional Mean / Std (mm)	Conventional (envelope) Mean / Std (mm)	UDD Mean / Std (mm)	UDD + Triangle Mean / Std (mm)
1	12.30 / 0.51	9.04 / 0.86	0.00 / 1.00	0.00 / 1.00
2	2.28 / 0.50	4.28 / 0.87	0.79 / 0.93	0.79 / 0.93
3	2.47 / 0.51	6.09 / 0.65	0.22 / 0.91	0.22 / 0.91
4	2.67 / 2.02	8.04 / 0.57	0.83 / 2.99	0.42 / 0.87

Fig. 6(c) and Table III indicate that all the calculated coordinates for each microphone were clustered into their respective bunches, with no large dispersed errors in UDD + Triangle. Here, the larger errors observed for mic 4 in UDD were eliminated, whereas the errors in UDD and UDD + Triangle for the other microphones were exactly the same. These results demonstrate that the triangle constraint was effective in overcoming the λ leap problem without degrading the accurate results obtained by discarding unreliable data.

C. Evaluation II: Multipath Interference

The effectiveness of the proposed technique in overcoming the multipath problem was also evaluated. For this evaluation, the experimental data were obtained at exactly the same locations as those in Fig. 6, except that the sound-absorbing fiber was removed. Then, the same three measurements as in Fig. 6 – Conventional, UDD, and UDD + Triangle – were performed, but this time, the maximum number of peaks picked from one *Tx–Rx* cross correlation was increased to four, considering the assumed worst case, that is, all three peaks – the highest multipath peak, its one-λ adjacent peak, and the λ leap of the direct path peak – have a higher value than the direct path peak. The positioning results of the three models are shown in Fig. 7. The true positions were the same as those in Fig. 6.

The most notable difference between Evaluations I and II is the result of mic 2, which is severely affected by multipath interference. In Fig. 7(a), in addition to the dispersed errors for mics 1 and 4, which are also observed in Fig. 6(a), large dispersed errors are also present, owing to multipath interference for mic 2 exceeding the plot range of the graph. In Fig. 7(b), the large mean errors outside the plot range for mic 2 remain along with some dispersed errors for mic 4, whereas none of these dispersed errors are present in Fig. 7(c). The errors shown in Fig. 7 are presented in Table IV. The results shown in Fig. 6 and 7 and Tables III and IV indicate that the proposed technique is an effective countermeasure to both λ-leap and multipath interference.

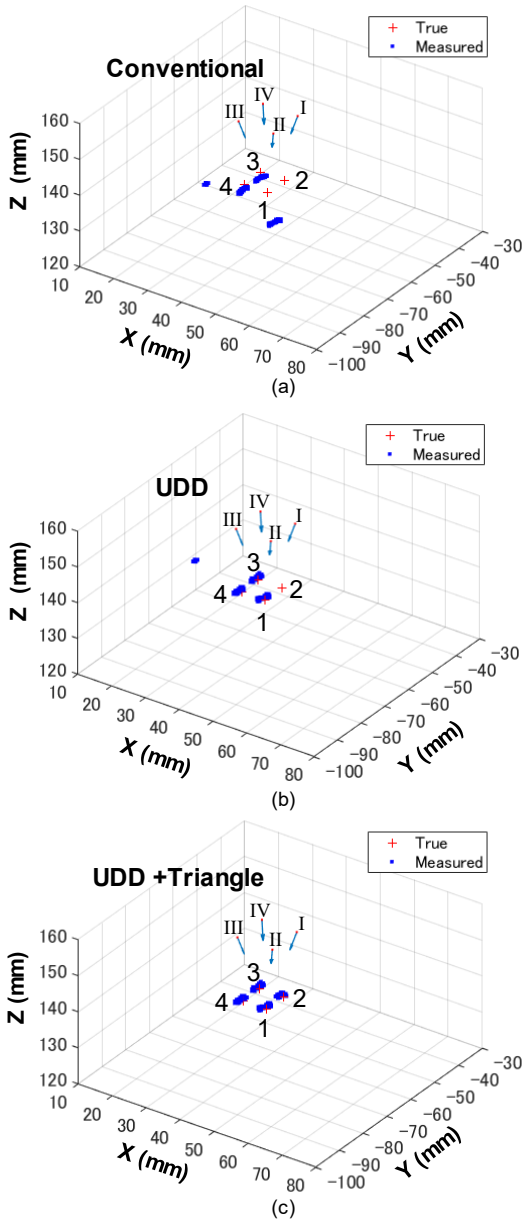

Fig. 7. Evaluation II: Multipath interference. In (a) Conventional and (b) UDD, the positions of mic 2 are outside the plot range. The results for mics 1 and 4 in (b) UDD are improved from (a) Conventional, which was also confirmed in Fig. 6. In (c) UDD + Triangle, no dispersed errors are observed.

TABLE IV
LOCATION ERRORS IN EVALUATION II: MULTIPATH INTERFERENCE

Mic.	Conventional Mean / Std (mm)	UDD Mean / Std (mm)	UDD + Triangle Mean / Std (mm)
1	12.02 / 1.20	1.04 / 1.21	1.04 / 1.21
2	1988.1 / 12133.7	820.12 / 1.23	1.32 /0.90
3	2.18 / 1.03	0.94 / 1.11	0.94 / 1.11
4	3.50 / 3.88	3.78 / 5.81	0.77 / 1.04

D. Evaluation III: 3-D Positioning Precision

Next, the 3-D positioning precision of the proposed technique was evaluated. For this evaluation, 124 measurements were taken at 11 locations within the movable range of the robot arm at every 14.14 mm step, which corresponded to a horizontal movement of 10 mm and a vertical movement of 10 mm in the robot arm coordinates. The measured results with the microphone combination (4, 1, 2) are plotted in Fig. 8.

The true positions marked by '+' in the figure were calculated through linear extrapolation using the mean coordinates of the first measurement from each microphone (the three lower left

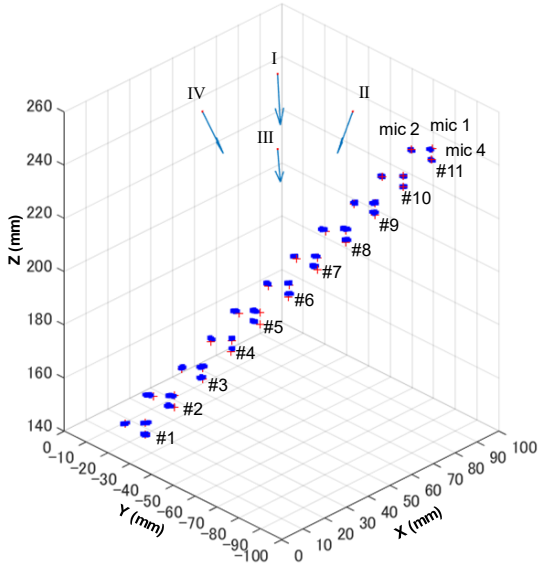

Fig. 8. 3-D Positioning precision: The 3-D positioning precision was evaluated at 11 positions by moving the robot arm 10 mm horizontally and 10 mm vertically at every step using the triangle constraint with the mic group (4, 1, 2).

dots) as the calibrated offset points and the step movement vector of the robot arm. The arrows I–IV indicate the direct paths from the corresponding transducers to mic 1 at position 6.

As shown in the figure, the measured results are in good agreement with the actual rectangular triangles at all locations. We also confirmed that the measurement results were the same regardless of the microphone combination.

Fig. 9. shows the location error for each measurement. On the horizontal axis, position 1 corresponds to the aforementioned calibration point. The error bar in the figure indicates the $\pm 1\sigma$ error range. No large dispersed errors were observed at any of the 33 measurement points. The errors were distributed within a range of less than ±1.21 mm.

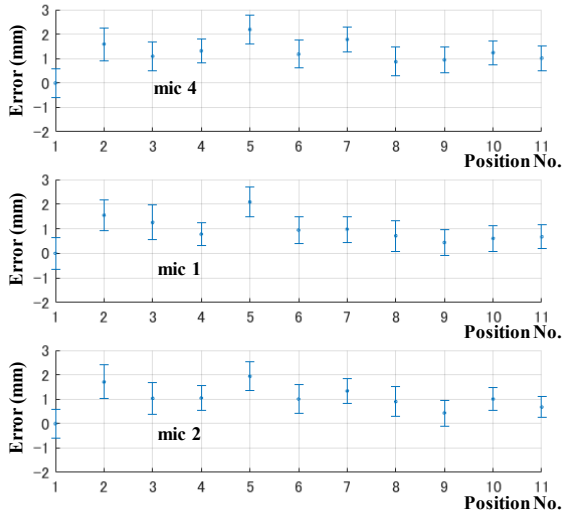

Fig. 9. 3-D Positioning errors. No large dispersed errors were observed at all the 33 measured points corresponding to 3 microphones × 11 positions.

Fig. 8 and 9 indicate that the proposed technique can measure the 3-D position with precision on the same order as that in the 1-D range measurement achieved in our previous study [20].

E. Evaluation IV: Detection Probability

Finally, the detection probability of the proposed technique under severely realistic conditions was evaluated. In this evaluation, a mic-array PCB was placed at 18 locations near the mocked room corner made by combining three acrylic panels, and the same measurements using microphones (4, 1, and 2) as in Evaluation III were taken. The dimensions of the mocked corner were 600 mm × 600 mm × 600 mm. The corner was placed near the position where the robot arm was originally set in Evaluations I–III, such that the three panels of the corner were set in parallel with the X-Z, Y-Z, and X-Y planes of the evaluation environment. Further, the direct paths from the four transducers to the microphones were not completely blocked, which is a necessary condition for the triangle constraint. The experimental setup for Evaluation IV is shown in Fig. 10. The mic-array PCB was placed at nine locations in one X-Y measurement plane. The X-Y measurement plane was also changed in two positions by changing the length of the pillars that supported the mic-array PCB. The PCB placement spans in the X, Y, and Z axes were 100, 100, and 105 mm, respectively.

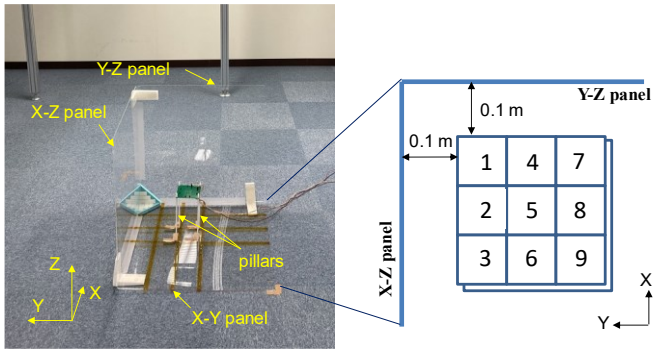

Fig. 10. Experimental environment for detection probability: The measurement was taken at 18 locations near the mocked room corner. The placement spans in X, Y, and Z axes were 100, 100, 105 mm, respectively.

The measured results are shown in Fig. 11. The symbols '+' in the figure show the reference positions of each measurement location, which were obtained from the mean measured coordinates at position 5 and a placement span of (100, 100, 105). The arrows I–IV indicate the direct paths from the corresponding transducers to mic 1 at position 5. The circles in the figure indicate the positions where the positioning calculations with the triangle constraint for all three microphones were successful, with a standard deviation of less than ± 2 mm throughout all 124 measurements.

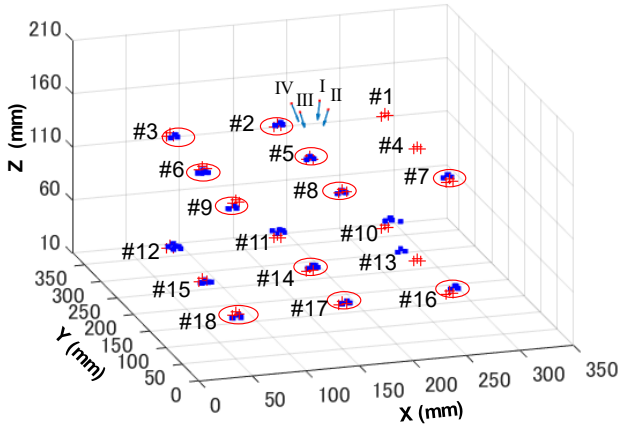

Fig. 11. Detection probability: Successful measurements with less than 2 mm standard deviation throughout all the 124 measurements were achieved at positions marked with a circle, whereas no positioning results with the triangle constraint were available at #1 and #4.

The detection probabilities and the worst standard deviations of the three microphones at other positions are listed in Table V. We have also confirmed that the detection probabilities in Fig. 6(c), Fig. 7(c) and in Fig. 8 were all 100 %.

TABLE V
DETECTION PROBABILITIES AND STANDARD DEVIATIONS: UNSUCCESSFUL LOCATIONS

Position	#1, #4	#10	#11	#12	#13	#15
Detection probability (%)	0	57.3	58.9	100	7.26	100
Std (mm)	-	6.53	1.82	8.59	0.46	9.40

F. Analysis

Fig. 12 shows the cumulative error distribution function (CDF) plots of the three distinctive positions and all the measurements from Fig. 11. The solid line (a) is the CDF with the least standard deviation of all measurements, which was observed at mic 4 at position 17. The dashed line (b) is the largest standard deviation among the successful locations marked by a circle in Fig. 11, which is given by mic 2 at position 14. The dotted line (c) shows the CDF, where the largest standard deviation was observed among all possible measurements in Evaluation IV, which was from mic 2 at position 15. The line (d) is that of all the microphones at all positions except for positions 1 and 4. The error in Fig. 12 was defined as the deviation of each measurement from the mean value. The jump from approximately 8 mm to 11 mm in (c) indicates the occurrence of dispersed errors, but they were not the type of large outliers affected by multipath interference as those for mic 2 of Conventional or UDD in Table IV. There were also other locations, such as positions 10 and 12 listed in Table V, where dispersed positioning errors were observed. However, at these locations, there were no dispersed errors larger than those of line (c), which is also confirmed by the fact that line (c) showed the worst error distribution of all.

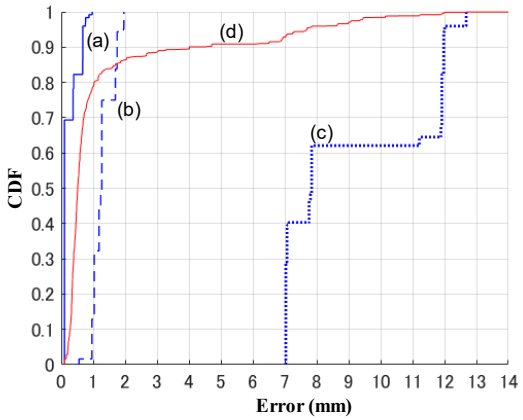

Fig. 12. Cumulative error distribution functions (CDF): Error distributions at three distinctive positions with (a) the least standard deviation of all, (b) the largest standard deviation among successful measurements, (c) the largest standard deviation of all the possible measurements and (d) the CDF of all the measurements except for positions 1 and 4.

V. Discussion

In all the evaluations, the mic-array PCB was placed almost parallel to the ceiling, where the four transducers were fixed. When the receiver surface is tilted, two problems must be considered. One is the phase ambiguity that occurs when the signal travelling path difference between adjacent microphones exceeds half the wavelength. However, in our proposal, this would not induce a serious problem because of the M-sequence's characteristic that its autocorrelation coefficient shows only one acute peak in the time axis, as shown in Fig. 1, which significantly suppresses the amplitude of $\pm N\ \lambda$ apart ghost peaks. Another possible problem is the signal attenuation depending on the directivity of the microphone. Attention should be paid to this in future practical applications, although it would not be a critical issue as long as omnidirectional microphones, as listed in Table I in our evaluation, are employed.

Another consideration for real applications is synchronization between the transmitters and receivers. As the synchronization error is regarded as one of the ranging errors, it should be suppressed to less than 10 μs to achieve 3.4 mm precision, for example. One solution to this problem is to employ radio frequency synchronization, as presented in [12]. Another option is to calculate the synchronization error together with the position coordinates, as performed in GPS, which is possible as long as all the transmitters are synchronized with sufficient precision, as in a wired transmitter system.

Although we understand that other error factors such as ambient noise or temperature drift also have to be addressed, and even a wider measurable range is required in future commercial IPS applications, such as human/pet/robot positioning systems, these issues will be the focus of future work. We assume that the calibration technique is promising for the former issue, whereas a wideband ultrasound transducer with a wider directivity is needed for the latter.

VI. Conclusion

A precise 3-D ultrasonic measurement technique using DSSS-CDMA was proposed. The proposed technique, which uses three microphones, was evaluated experimentally. High precision was achieved in 3-D positioning by constraining the transmitter and its two adjacent receivers to form the vertices of a triangle. The standard deviation was less than 1.21 mm, and there were no dispersed errors caused by multipath interference in the field, thus avoiding the need to employ interference-compensating signal processing, such as PIC. Because of its precise, robust, and simple characteristics, the proposed technique is suitable for potential future IPS applications, such as autonomous driving drones/robots, pets, indoor sports motion analysis, and other applications where precise positioning with a precision higher than 1 cm is required.

References

[1] G. M. Mendoza-Silva *et al.*, "A meta-review of indoor positioning systems," *Sensors (Basel)*, vol. 19, no. 20, pp. 4507–4551, 2019 [DOI: 10.3390/s19204507].

[2] M. Hazas and A. Ward, "A novel broadband ultrasonic location system," in *Lect. Notes Comput. Sci. Intl. Conf.* on Ubiquitous Comput. Berlin, Heidelberg. Springer, pp. 264–280, 2002 [DOI: 10.1007/3-540-45809-3_21].

[3] M. Hazas and A. Hopper, "Broadband ultrasonic location systems for improved indoor positioning," *IEEE Trans. Mob. Comput.*, vol. 5, no. 5, pp. 536–547, 2006 [DOI: 10.1109/TMC.2006.57].

[4] J. C. Prieto *et al.*, "Subcentimeter-accuracy localization through broadband acoustic transducers" in *IEEE Intl. Symp. Intell. Signal Process.*, vol. 2007, pp. 1–6, 2007.

[5] J. C. Prieto *et al.*, "Performance evaluation of 3D-LOCUS advanced acoustic LPS," *IEEE Trans. Instrum. Meas.*, vol. 58, no. 8, pp. 2385–2395, 2009 [DOI: 10.1109/TIM.2009.2016378].

[6] C. Sertatıl *et al.*, "A novel acoustic indoor localization system employing CDMA," *Digit. Signal Process.*, vol. 22, no. 3, pp. 506–517, 2012 [DOI: 10.1016/j.dsp.2011.12.001].

[7] M. C. Perez *et al.*, "Performance comparison of different codes in an ultrasonic positioning system using DS-CDMA" in *IEEE Intl Symp. on Intell. Signal Process.*, vol. 2009, pp. 125–130, 2009.

[8] F. Seco *et al.*, "Compensation of multiple access interference effects in CDMA-based acoustic positioning systems," *IEEE Trans. Instrum.*

Meas., vol. 63, no. 10, pp. 2368–2378, 2014 [DOI: 10.1109/TIM.2014.2312511].
[9] F. Seco *et al.*, "Fine-grained acoustic positioning with compensation of CDMA interference" in *IEEE Intl. Conf. Ind. Technol. (ICIT)*, vol. 2015, pp. 3418–3423, 2015.
[10] C. Medina *et al.*, "Ultrasound indoor positioning system based on a low-power wireless sensor network providing sub-centimeter accuracy," *Sensors (Basel)*, vol. 13, no. 3, pp. 3501–3526, 2013 [DOI: 10.3390/s130303501].
[11] J. Zhao and Y. Wang, "Autonomous ultrasonic indoor tracking system." in *IEEE Intl. Symp. Parallel Distrib. Process. Appl*, vol. 2008, 2008, pp. 532–539.
[12] R. Carotenuto *et al.*, "An indoor ultrasonic system for autonomous 3-D positioning" *IEEE Trans. Instrum. Meas.*, vol. 68, no. 7, pp. 2507–2518, 2019 [DOI: 10.1109/TIM.2018.2866358].
[13] J. R. Gonzalez and C. J. Bleakley, "High-precision robust broadband ultrasonic location and orientation estimation," *IEEE J. Sel. Top. Signal Process.*, vol. 3, no. 5, pp. 832–844, 2009 [DOI: 10.1109/JSTSP.2009.2027795].
[14] M. Alloulah and M. Hazas, "An efficient CDMA core for indoor acoustic position sensing" in *Intl. Conf. Indoor Position. Indoor Navig. (IPIN)*, vol. 2010. IEEE, 2010, pp. 1-5.
[15] J. A. Paredes *et al.*, "Analysis of Doppler effect on the pulse compression of different codes emitted by an ultrasonic LPS," *Sensors (Basel)*, vol. 11, no. 11, pp. 10765–10784, 2011 [DOI: 10.3390/s111110765].
[16] Y. Itagaki *et al.*, "Indoor positioning for moving objects using a hardware device with spread spectrum ultrasonic waves" in *Intl. Conf. Indoor Position. Indoor Navig. (IPIN)*, vol. 2012, pp. 1–6, 2010.
[17] F. J. Álvarez *et al.*, "Doppler-tolerant receiver for an ultrasonic LPS based on Kasami sequences," *Sens. Actuators A,* vol. 189, pp. 238–253, 2013 [DOI: 10.1016/j.sna.2012.09.029].
[18] F. J. Álvarez *et al.*, "CDMA-based acoustic local positioning system for portable devices with multipath cancellation," *Digit. Signal Process.,* vol. 62, pp. 38–51, 2017 [DOI: 10.1016/j.dsp.2016.11.001].
[19] S. Hirata *et al.*, "Evaluation of position and velocity measurement for a moving object by pulse compression using ultrasound coded by preferred-pair M-sequences" in *IEEE Int. Ultrason. Symp. (IUS)*. IEEE, 2017, pp. 1–4.
[20] T. Ishii *et al.*, "Subcentimeter precision ranging system for moving targets with a doppler-effect-compensated ultrasonic direct sequence spread spectrum," *IEEE Trans. Instrum. Meas.*, vol. 70, pp. 1–8, 2020.
[21] A. Goldsmith, *Wireless Communications*. *Cambridge University Press*, 2005.
[22] A. Weiss and E. Weinstein, "Fundamental limitations in passive time delay estimation – Part II: Wid-band systems," *IEEE Trans. Acoust., Speech, Signal Process*., vol. ASSP-32, no. 5, pp. 1064–1078, Oct. 1984.
[23] Y. He and A. Bilgic, "Iterative least squares method for global positioning system," *Adv. Radio Sci.*, 9(C.5-2) pp. 203–208, 2011.
[24] H. Liu *et al.*, "Survey of wireless indoor positioning techniques and systems," *IEEE Trans. Syst. Man Cybern. C (Applications and Reviews),* vol. 37, no. 6, pp. 1067–1080, 2007 [DOI: 10.1109/TSMCC.2007.905750].

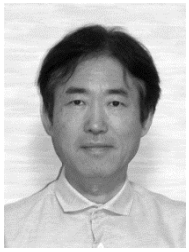

ISHII Toru received a B. Eng. degree in electronic engineering from Kyoto University, Kyoto, Japan, in 1986, and an MBA degree from Kobe University, Kobe, Japan, in 2013. He joined Minolta, Osaka, Japan, in 1986, where he developed digital imaging devices. He moved to Murata Manufacturing, Kyoto, Japan, in 1999, where he was a development manager for automotive radars, communication modules, and sensors. Since 2018, he has been engaged in research on ultrasound sensing as a postgraduate student at Kobe University.

Yuto Yasuda received a B. Eng. degree in Computer Science and Systems Engineering from Kobe University, Kobe, Japan in 2021. He is currently in the master's course at Kobe University. His current research is environmental sensing using an ultrasonic array sensor.

Shun Sato received a B. Eng. degree in Computer Science and Systems Engineering from Kobe University, Kobe, Japan in 2022. He is currently in the master's course at Kobe University. His current research is environmental sensing using an ultrasonic array sensor.

Shintaro Izumi (S'09- M'12) received his B. Eng. and M. Eng. degrees in Computer Science and Systems Engineering from Kobe University, Kobe, Japan, in 2007 and 2008, respectively. He received his Ph.D. degree in Engineering from Kobe University in 2011. He was a JSPS research fellow at Kobe University from 2009 to 2011, an Assistant Professor in the Organization of Advanced Science and Technology at Kobe University from 2011 to 2018, and an Associate Professor at the Institute of Scientific and Industrial Research at Osaka University from 2018 to 2019. Since 2019, he has been an Associate Professor at the Graduate School of System Informatics, Kobe University, Japan. His current research interests include biomedical engineering, biosignal processing, low-power circuit design, and sensor networks.
He has served as a Technical Committee Member for IEEE Biomedical and Life Science Circuits and Systems, as a student activity committee member for the IEEE Kansai Section, and as a Program Committee Member for the IEEE Symposium on Low-Power and High-Speed Chips (COOL Chips). He was a Chair of the IEEE Kansai Section Young Professionals Affinity Group and a recipient of the 2010 IEEE SSCS Japan Chapter Young Researchers Award.

Hiroshi Kawaguchi (M'98) received B. Eng. and M. Eng. degrees in electronic engineering from Chiba University, Chiba, Japan, in 1991 and 1993, respectively, and earned a Ph.D. degree in electronic engineering from the University of Tokyo, Tokyo, Japan, in 2006.
He joined Konami Corporation, Kobe, Japan, in 1993, where he developed arcade entertainment systems. He moved to the Institute of Industrial Science, University of Tokyo, as a Technical Associate in 1996, and was appointed as a Research Associate in 2003. In 2005, he moved to the Graduate School of Engineering, Kobe University, Kobe, Japan, as a Research Associate. From 2015 to 2016, he was a Visiting Researcher at Politecnico di Milano. Since 2016, he has been a Full Professor at the Graduate School of Science, Technology, and Innovation at Kobe University. He is also a Collaborative Researcher at the Institute of Industrial Science at the University of Tokyo. His current research interests include low-power operating circuits, memory circuits, sensing systems, signal processing, and machine-learning hardware.
Dr. Kawaguchi was a recipient of the IEEE ISSCC 2004 Takuo Sugano Outstanding Paper Award, ACM/IEEE ASP-DAC 2013 University Design Contest Best Design Award, and IEEE ICECS 2016 Best Paper Award. He has served as a Design and Implementation of Signal Processing Systems (DISPS) Technical Committee Member for the IEEE Signal Processing Society; as a Technical Program Committee Member for the IEEE International Conference on Acoustics, Speech and Signal Processing (ICASSP), IEEE Global Conference on Signal and Information Processing (GlobalSIP), IEEE Workshop on Signal

Processing Systems (SiPS), IEEE Custom Integrated Circuits Conference (CICC), and IEEE Symposium on Low-Power and High-Speed Chips (COOL Chips); as an Organizing Committee Member for the IEEE Asian Solid-State Circuits Conference (A-SSCC) and ACM/IEEE Asia and South Pacific Design Automation Conference (ASP-DAC); and as an Associate Editor of Springer Journal of Signal Processing Systems, IEICE Transactions on Fundamentals of Electronics, Communications and Computer Sciences, IEICE Transactions on Electronics, and IPSJ Transactions on System LSI Design Methodology (TSLDM).
He is a member of the IEEE, ACM, and IEICE.

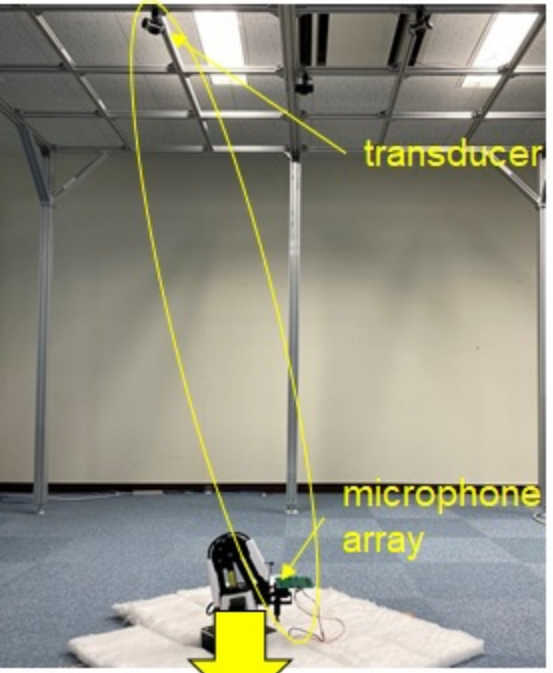
transducer
microphone
array

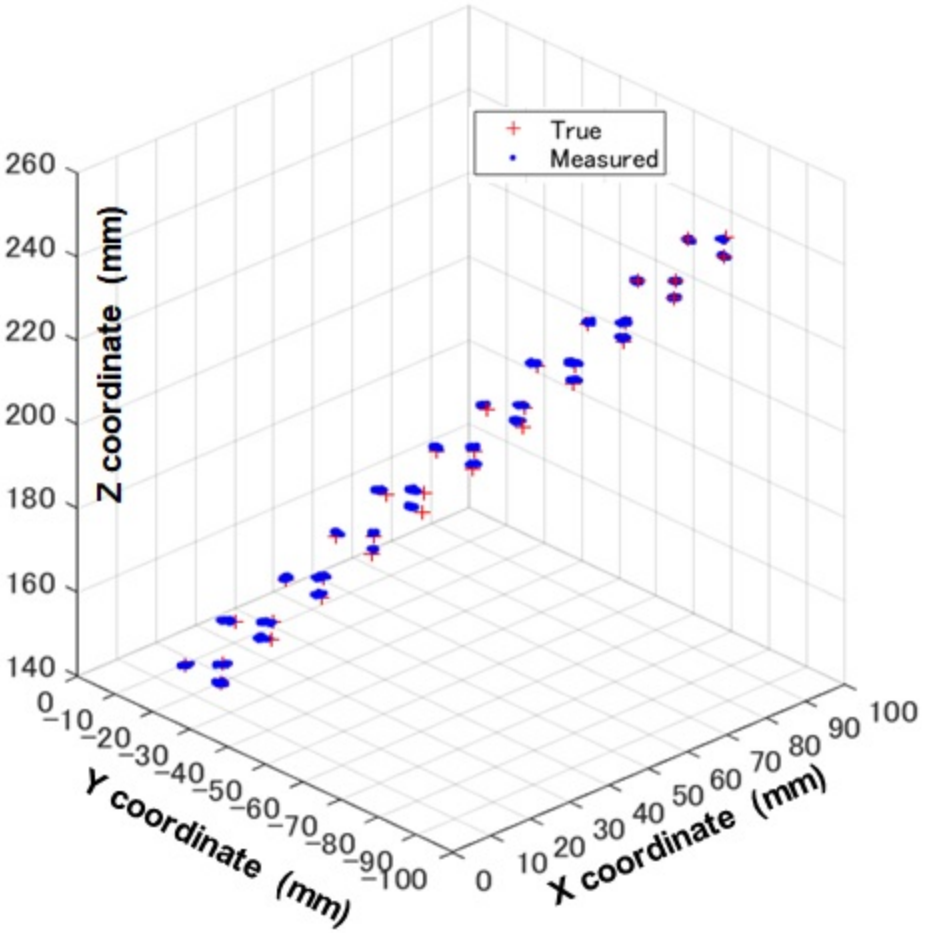
True
Measured
Z coordinate (mm)
260
240
220
200
180
160
140
Y coordinate (mm)
0
−10
−20
−30
−40
−50
−60
−70
−80
−90
−100
X coordinate (mm)
0
10
20
30
40
50
60
70
80
90
100

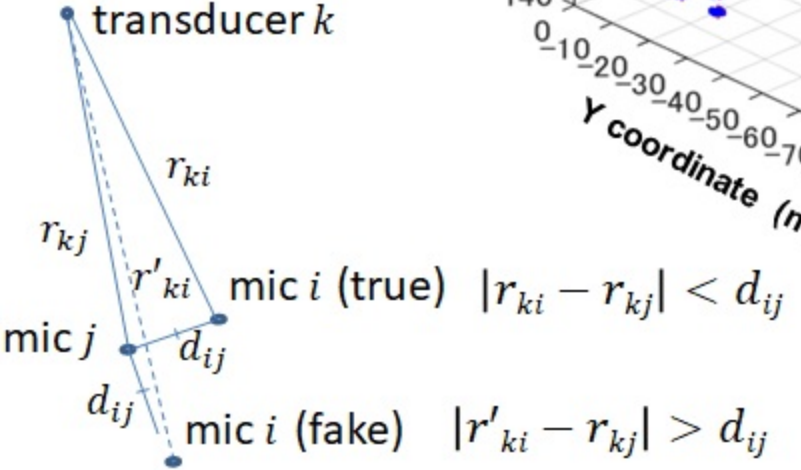
transducer k
r_{ki}
r_{kj}
r'_{ki}
mic i (true) $|r_{ki} - r_{kj}| < d_{ij}$
mic j
d_{ij}
d_{ij}
mic i (fake) $|r'_{ki} - r_{kj}| > d_{ij}$